Published in final edited form as:
J Magn Reson. 2012 July ; 220: 94–101. doi:10.1016/j.jmr.2012.04.012.

A Large Volume Double Channel ^{1}H-X RF Probe for Hyperpolarized Magnetic Resonance at 0.0475 Tesla

Aaron M. Coffey[1,2], **Roman V. Shchepin**[1], **Ken Wilkens**[1], **Kevin W. Waddell**[1], and **Eduard Y. Chekmenev**[1,2]

[1]Institute of Imaging Science, Department of Radiology, Vanderbilt University, Nashville, TN 37232

[2]Department of Biomedical Engineering, Vanderbilt University, Nashville, TN 37235

Abstract

In this work we describe a large volume 340 mL ^{1}H-X magnetic resonance (MR) probe for studies of hyperpolarized compounds at 0.0475 T. ^{1}H/^{13}C and ^{1}H/^{15}N probe configurations are demonstrated with the potential for extension to ^{1}H/^{129}Xe. The primary applications of this probe are preparation and quality assurance of ^{13}C and ^{15}N hyperpolarized contrast agents using PASADENA (parahydrogen and synthesis allow dramatically enhanced nuclear alignment) and other parahydrogen-based methods of hyperpolarization. The probe is efficient and permits 62 μs ^{13}C excitation pulses at 5.3 Watts, making it suitable for portable operation. The sensitivity and detection limits of this probe, tuned to ^{13}C, are compared with a commercial radio frequency (RF) coil operating at 4.7 T. We demonstrate that low field MR of hyperpolarized contrast agents could be as sensitive as conventional high field detection and outline potential improvements and optimization of the probe design for preclinical *in vivo* MRI. PASADENA application of this low-power probe is exemplified with ^{13}C hyperpolarized 2-hydroxyethyl propionate-1-^{13}C,2,3,3-d_3.

Keywords

hyperpolarization; multi-nuclear; magnetic resonance probe; parahydrogen; ^{13}C; ^{15}N; low field

1. Introduction

We have recently demonstrated *in situ* detection of parahydrogen induced polarization (PHIP) using Parahydrogen And Synthesis Allow Dramatically Enhanced Nuclear Alignment (PASADENA) [1; 2] in a 0.0475 T permanent magnet equipped with a 60 mL reactor inside a dual resonance NMR circuit [3; 4]. In *situ* detection facilitates quality assurance (QA) of PHIP experiments in general [4] and is useful for identifying optimal preparation parameters in studies of new hyperpolarized contrast agents [3]. In this work we present a significant improvement of the RF circuit performance by dividing it into two separate channels ^{1}H and X with individual transmit-receive coils. This separation allows for improved MR sensitivity on the X channel, which is essential for *in situ* detection of small quantities of hyperpolarized contrast agents.

Low resonance frequencies offer some unique opportunities for RF coil design, because the long conductors can be used to make multi-turn inductors. These conductor lengths are possible due to the long wavelengths at low frequencies [5]. For example, λ/10 = 60 meters

Correspondence: E. Chekmenev, Institute of Imaging Science, Department of Radiology, Vanderbilt University, Nashville, TN 37232 Fax: +1 (615) 322-0734 eduard.chekmenev@vanderbilt.edu.

at 0.5 MHz corresponding to the ^{13}C resonant frequency at 0.0475 T. Moreover, the signal voltage detected by NMR [6; 7], or electromotive force (*Emf*) arising from Faraday's law of induction, is linearly proportional to the number of turns (N) and the change of magnetic flux φ_B through a single loop, or $|Emf| = N \cdot |\Delta\varphi B/\Delta t| = N \cdot S \cdot |\Delta_B/\Delta t|$, where S is surface area through which the magnetic field B passes. Moreover, it can also be expressed as $|Emf| \propto N \cdot \omega_0 \cdot P \cdot \mu$, where ω_0 is the resonant frequency, P is the nuclear spin polarization, and μ is the magnetic moment of nuclear spin. Using multi-turn inductors in high field MR faces the primary limitations of (i) conductor length limitations according to $\lambda/10$ wavelength, (ii) parasitic effects related to eddy currents, (iii) self resonance frequency and (iv) dielectric losses associated with the conservative electric field E_C which is linearly proportional to the number of turns and the magnetic field, $E_C \propto N \cdot B_0$ [8]. The latter was discussed in detail by Gor'kov, P. L. and Brey W. W. in work on low-E resonators [8; 9]. In view of these constraints it proves advantageous to use single turn inductors for high field *in vivo* and ultra-high field *in vitro* work. On the other hand, all of the above limitations except for inductor self-resonance strongly correlate with field strength, scaling either linearly or with significant reduction with respect to the resonant frequency ω_0. It follows that the reduction in *Emf* due to ω_0, can be offset by increasing the number of turns in the detection MR coil. As a result of this compensation, low frequency RF coils can potentially approach the sensitivity of high field ones to the extent that the product $N \cdot \omega_0$ can be maintained nearly constant.

Low magnetic field MR and Earth field MR is an active and promising area of research [10] [11; 12; 13; 14; 15]. While the above basic principle to attain high sensitivity at low field is promising, there are a few challenges related to low field MR. First, the low chemical shift dispersion in units of Hz limits the majority of applications that are otherwise available in the high field regime. Second, the above argument does not take into account the noise and as a result signal-to-noise (SNR). Most important, however, the dominant penalty relates to intrinsic nuclear spin polarization P, which also scales linearly with applied magnetic field. As a result of this diminished magnetic flux, conventional low field MR is doomed to have significantly lower sensitivity based on the *Emf* argument described here.

However, emerging hyperpolarized technologies allow for preparation of nuclear spin states, when polarization levels become extrinsic to the static B_0 field. Specifically, if hyperpolarized spin states are detected, their nuclear spin polarization is independent of the applied magnetic field and their resonance frequency ω_0. Therefore, the magnetic field B is approximately field independent and the induced *Emf* with multi-turn resonators using low B_0 field should provide a sensitive means for MR detection of hyperpolarized compounds. This approach is demonstrated here for ^{13}C and ^{15}N at 0.0475 T and compared to high field ^{13}C detection at 4.7 T. Limitations and potential improvements are discussed and low field MR of hyperpolarized contrast agents compared to conventional detection at high field.

Although the noise consideration is necessary for a complete understanding of SNR, this is outside the scope of this work. We only point out that dielectric losses dominate MR noise for high field *in vivo* MRI of conductive Boltzmann polarized samples and that $SNR \propto \omega$, while the scaling rule applicable to non-conductive Boltzmann polarized samples in low field MR is $SNR \infty \omega^{7/4}$ [16]. In view of this there could be additional *RF* benefits for low field detection of hyperpolarized compounds. Moreover, there could be a SNR maximum at a particular resonant frequency for a specific coil geometry, subject size and properties [17].

^{13}C and ^{15}N hyperpolarized compounds can be prepared by various processes such as Dynamic Nuclear Polarization (DNP) [18] and PHIP. One of their most promising applications is their use as contrast agents to interrogate metabolism on second and minute time scales in living organisms. There are several key advantages of these contrast agents -

they are non-radioactive, allow for sub-second imaging speed [19], exhibit fast uptake which translates to a short wait time, and their rapid clearance potentially enables same-day follow-up scan(s) [20]. Other benefits of hyperpolarized MRI contrast agents include relatively low toxicity and many are already approved for use in their non-hyperpolarized form.

Despite clear advantages to hyperpolarized MRI, clinical implementation of this advanced technology hinges on two critical developments in the field: the ability to produce short-lived contrast agents on site and the capacity to perform efficient MRI of these agents [21]. Low field heteronuclear MRI using the antennas presented here may provide significant advantages for detection of hyperpolarized contrast agents in animals and humans due to MRI scanner cost reduction and increased patient safety due to low specific absorption rate (SAR). Moreover, negligible magnetic field susceptibility using fields below 0.05 T may eliminate time-consuming magnetic field shimming for MRI exams providing a unique possibility to accomplish the entire imaging examination in less than a second. In addition, it could be possible to devise highly portable low field imaging devices or/and MRI scanners compatible with other imaging modalities such as Computed Tomography (CT).

2. Methods

2.1 RF Circuit

Because low magnetic field is generated by a permanent magnet configured in a Halbach array with B_0 = 0.0475 T (Magritek, Wellington, New Zealand) used herein, it is possible to align B_0 perpendicular to the magnet bore thereby allowing for using large volume, multi-turn solenoid RF coils to maximize NMR sensitivity (Fig. 1). The second channel's RF coil is implemented using a multi-turn dual saddle shaped coil for the ^{1}H channel. The B_1 alternating fields of the two RF coils are orthogonal to B_0 and additionally to each other for RF isolation (Fig. 1).

A dual channel NMR probe has two separate RF coils with two independent tuning and matching circuits. The maximum length of wire was adjusted so as to enable the inductor self-resonance frequency to be higher than the Larmor frequency for each RF coil. The RF circuit shown in Fig. 2A consists of two single channel circuits sharing a ground with capacitors for achieving suitable tuning range and impedance matching for ^{1}H and X channels (X = ^{13}C or ^{15}N). The NMR probe frequencies of interest are 2.02 MHz (^{1}H), 0.508 MHz (^{13}C), and 0.205 MHz (^{15}N) at B_0 = 0.0475 T. The ^{1}H circuit consists of an outer 70 mm × 130 mm (I.D. × length) Helmholtz saddle coil. The second X channel coil is a 50 mm × 170 mm (I.D. × length) single layer solenoid closely fitted to the high-pressure reactor used for molecular addition of parahydrogen to unsaturated molecular precursors. The RF circuit tuning and matching networks were constructed from fixed C22CF series capacitors (Dielectric Laboratories, Cazenovia, NY) used in parallel with variable capacitors (model NMTM120C, Voltronics, Denville, NJ). The capacitor component values are given in Table 1. Switching from ^{13}C frequency to ^{15}N operation is achieved by adding fixed capacitors to the tune and match. Air core inductors were wound from 20 AWG magnet wire to form both RF coils. Inductances were measured with an Agilent E5071C network analyzer. The 16 turn (8 on each side) Helmholtz saddle coil and 206 turn solenoid produced L_H = 40 μH and L_X = 550 μH, respectively (see Fig. 2C). The solenoid wire length was 34 meters, which is below λ/10 at ^{13}C and ^{15}N Larmor frequencies.

2.2 RF Pulse Calibration

RF pulse width was calibrated using two different methods: complete nutation curve by incrementing pulse width or in the case when Boltzmann polarization was too low to yield sufficient SNR, the sample was pre-polarized using a high field magnet [11] and single scan spectra were used to determine $\tau_{90°}$ and $\tau_{180°}$. Pre-polarization of phantoms at high field (4.7 T and 7 T) enhances nuclear spin polarization by 100 fold or more compared to that at 0.0475 T. As a result, the detected signal at 0.0475 T from such pre-polarized phantoms can be increased by 100+ fold [11] to allow for single scan sensitivity. Because NMR SNR scales with the square root of the number of signal averages, it would therefore take 10,000 averages to achieve the same sensitivity. This is impractical with repletion times in excess of two minutes for ^{13}C and ^{15}N. For example, the Boltzmann thermal equilibrium ^{13}C polarization is $P = 6.04\times10^{-6}$ at 7 T and 298 K and it decays to $P \sim 4\times10^{-6}$ during 7-second long sample transfer from 7 T magnet into a 0.0475 T magnet according to spin lattice relaxation time ^{13}C T_1 of in sodium 1-^{13}C-acetate, see below. This is in quantitative agreement with our experimental observations that externally induced 4.06×10^{-6} polarization is ~100 fold greater than Boltzmann ^{13}C polarization $P = 4.06\times10^{-8}$ at 0.0475 T. The high SNR allows accurate determination of $\tau_{90°}$ to within 1 μs corresponding to < 2% angular error. When a 90° excitation pulse is used the first scan results in maximum signal intensity, while the successive scan acquired within a few seconds after the first one (T_1 >> TR), yields nearly zero signal intensity. When 180° excitation pulse is used, almost no signal is detected. Because B_0 susceptibility and B_1 homogeneity are essentially independent of the sample load at such low field, once RF pulses are calibrated, the calibrated $\tau_{90°}$ values were used for all other samples and MR experiments. An automated routine supplied by the Kea^2 spectrometer manufacturer (Magritek, Wellington, New Zealand) was used for RF pulse length calibration, which increments pulse duration at constant power. A ^{1}H nutation curve was recorded using a 24 mL spherical phantom of deionized H_2O with 5 mM $CuSO_4$ (T_1 < 0.1 s). A 60 mL spherical phantom containing 14 g of sodium 1-^{13}C-acetate in 56 g 99.8% D_2O was used for ^{13}C pulse calibrations and as a reference ^{13}C signal for estimating % polarization (see Results). INEPT (Insensitive Nuclei are Enhanced by Polarization Transfer) [22] was therefore used to transfer the magnetization from more polarized methyl protons to ^{13}C in the 1-^{13}C-acetate phantom, increasing ^{13}C polarization by ~3.5 fold and significantly decreasing repetition time (TR) from 200 s to 10 s. Generating automated nutation curves with INEPT allowed for overnight ^{13}C pulse calibrations. A 48 mL spherical phantom with 12 g of $^{15}NH_4Cl$ in 99.8% D_2O was used for ^{15}N RF pulse calibrations.

2.3 NMR Spectroscopy

All NMR spectra were recorded with a 10 kHz spectral width. For experiments at 0.0475 T, the spectra were recorded with 102.4 ms acquisition time and 1,024 sample points. For ^{13}C experiments at 4.7 T, a triple resonance ^{1}H/^{13}C/^{15}N RF coil (Doty Scientific, SC) was used with a 0.5 second acquisition time and 10 kHz spectra width.

2.4 ^{13}C longitudinal relaxation time T_1 of sodium 1-^{13}C-acetate phantom

1-^{13}C T_1 of the sodium 1-^{13}C-acetate in 99.8% D_2O phantom at Earth's field (~ 50 μT) and 0.0475 T were measured by pre-polarizing the phantom at B_0 = 3 T for 5 minutes before acquisition at B_0 = 0.0475 T with $\tau^{90°}$. Once the ^{13}C sample is removed from 3 T magnetic field, it is exposed to Earth field during its transfer to 0.0475 T for MR signal detection. The transfer time was incremented for Earth field ^{13}C T_1 measurements and maintained constant (20 ± 1 s) for 0.0475 T ^{13}C T_1 measurements. ^{13}C T_1 was measured by fitting an exponential signal decay as a function of incremented ^{13}C sample exposure to Earth (T_1 = 18.5 ± 0.8 s) and 0.0475 T (T_1 = 50.0 ± 2.6 s) fields respectively, (Fig. 4). These values were used for TR settings for ^{13}C direct detection of this ^{13}C reference phantom and for estimating polarization losses during sample transfer between high field (4.7 T) and low field (0.0475 T).

2.5 B_0 homogeneity

There are many low field magnet options currently available from several manufacturers including Bruker (Aspect Desktop MRI), MRTechnology (0.3 T MRI), Time-Medical (0.2 T and 0.35 T MRI) offering improved magnetic field homogeneity versus our 0.0475 T Halbach magnet. The 0.0475 T permanent magnet was manually shimmed with small 1/4" diameter × 1/16" thick neodymium magnets (D41-N52, KJMagnetics, Jamison, PA) to improve magnetic field homogeneity. Proper placement was determined by decreasing line full width at half maximum (FWHM). The ^{1}H FWHM of the 24 mL water phantom was approximately 20 Hz, or about 10 ppm after shimming (Fig. 3A). The Halbach array magnet was temperature stabilized at 35 °C to prevent any time-dependent B_0 field drift.

3. Results

3.1 B_1

The probe RF circuit frequency responses for ^{1}H, ^{13}C, and ^{15}N are shown in Fig. 2B. The quality factors of the RF circuits measured via Agilent E5071C network analyzer were Q = 38 for ^{1}H, Q = 80 for ^{13}C, and Q = 67 for ^{15}N. RF square pulse calibration yielded ^{1}H $\tau_{90°}$ = 86 μs (5.3 W) at 2.02 MHz, ^{13}C $\tau_{90°}$ = 62 μs (5.3 W) at 0.508 MHz, and ^{15}N $\tau_{90°}$ = 73 μs (10.5 W) at 0.205 MHz. Precise values of B_0 and ^{13}C and ^{15}N resonant frequencies were calculated from the experimentally measured proton frequency, scaled in accord to gyromagnetic ratios. The summary of $\tau_{90°}$ and corresponding B_1 is provided in Table 1. Fig. 3A shows a representative ^{1}H spectrum acquired with 90° excitation pulse. The spectra shown in Figs. 3B and 3C were acquired with a $\tau_{90°}$ excitation pulse using pre-polarization at 4.7 T and 7 T for ^{13}C and ^{15}N respectively and ~7 s sample transfer time from high to low field.

3.2 Parahydrogen Induced Polarization (PHIP) using PASADENA effect

HEP (2-hydroxyethyl propionate-1-^{13}C,2,3,3-d_3) was hyperpolarized with PASADENA [1; 2] by catalytic hydrogenation of HEA (2-hydroxyethyl acrylate-1-^{13}C,2,3,3-d_3, 676071, Sigma-Aldrich-Isotec, Miamisburg, OH) using up to 97 % enriched parahydrogen produced by an in-house semi-automated parahydrogen generator [23]. Experimental polarization procedures were similar to those previously described [4] except that deionized water was used instead of 99.8% D_2O as a solvent. Figs. 5B and 5C respectively demonstrate direct detection of the ^{13}C Boltzmann signal of a reference sample and *in situ* detection of ^{13}C hyperpolarized HEP. The signal with a 13C SNR ~ 2,300 and FWHM = 26 Hz is recorded from 15 micromoles (< 2 mg) of HEP with 20% polarization corresponding to signal and polarization enhancement ε ~ 5, 000, 000 (Fig. 5C).

The level of ^{13}C hyperpolarization was also measured as function of ^{1}H continuous wave decoupling power level in the Goldman PHIP polarization transfer sequence [24] to investigate the lower limit of RF power necessary to perform efficient PHIP and produce hyperpolarized agents. A significant reduction of ^{1}H decoupling power leads to a modest decrease in ^{13}C hyperpolarization (Fig. 6A). This is possible due to relatively good magnet B_0 and B_1 homogeneity that allows efficient RF excitation even at relatively very low power level. For example, the polarization level at 0.33 W is 86% of the maximum observed level at 10.5 W in these experiments. However, the polarization level at 0.08 W is only 66% of maximum value, which represent a significant hyperpolarization loss.

In a separate experimental series, the power level of decoupling and all ^{13}C and ^{1}H RF pulses of PHIP polarization transfer sequence was varied at the same time (Fig. 6B). Hyperpolarization levels at 0.66 W and 0.33 W decreased to 92% and 90.5% respectively compared to hyperpolarization obtained with 10.5 W RF power.

3.3 MR sensitivity at high and low field under conditions of constant nuclear spin polarization

The ^{13}C RF probe sensitivity was compared to that of a commercial 4.7 T small-animal RF coil with smaller volume. The 4.7 T equipment consisted of a Varian 4.7 T scanner and a 38 mm I.D. triple resonance RF volume coil from Doty Scientific, SC. The RF coils have similar diameter, but the 0.0475 T solenoid coil is ~ 2 times longer. The spherical phantom used for both instruments consisted of 1.0 g of sodium 1-^{13}C-acetate dissolved in 2.8 mL 99.8% D_2O. Equilibrium Boltzmann ^{13}C polarization at 298 K of P = 4.06×10^{-6} at 4.7 T and ^{13}C P = 6.04×10^{-6} at 7 T was achieved by phantom polarization for at least 5*T_1 . Equilibrium polarization P = 4.06×10^{-6} *1* was used for ^{13}C signal detection with $\tau_{90°}$ on the 4.7 T Varian MRI scanner. The ^{13}C phantom with ^{13}C P = 6.04×10^{-6} achieved at 7 T was transferred to the 0.0475 T low field system and ^{13}C signal was detected with $\tau_{90°}$. The sample transfer time of approximately 7 s delay resulted in ^{13}C polarization decay (^{13}C T_1 = 18.5 s at Earth field) from 6.04×10^{-6} *1* to ~4.0×10^{-6}. The latter value is within a few percent of the 4.7 T Boltzmann equilibrium level of 4.06×10^{-6}. Therefore, the ^{13}C phantom had nearly identical ^{13}C nuclear spin polarization when detected on 4.7 T and 0.0475 T MR systems simulating the conditions of the magnetic field independent hyperpolarized state. The 4.7 T RF volume coil yielded a SNR of 120 with a FWHM of 6 Hz (Fig. 7). The ^{13}C solenoid coil of the 0.0475 T H-X probe achieved an SNR of 28 with a FWHM of 25 Hz (Fig. 7). Therefore, the sensitivity of the two coils measured as a product of FWHM and SNR is approximately the same. We note that FWHM of the ^{13}C resonance in Fig. 7B is considerably narrower than that in Fig. 3B due to significantly smaller sample volume and significantly reduced effects of magnetic field inhomogeneity.

4. Discussion

A dual channel 0.0475 T PHIP H-X RF probe provides sufficient sensitivity to enable direct ^{13}C detection and excitation using Boltzmann polarized and hyperpolarized samples at 508 kHz. Direct ^{15}N detection at 205 kHz is somewhat less sensitive and sample pre-polarization at high field is required. The ability for direct low field NMR detection allows for an external calibration standard with known concentration, MR signal, and polarization. Direct calculation of polarization provides greater accuracy for quality assurance of hyperpolarization with such a reference standard. This convenient detection of ^{13}C polarization levels *in situ* does not require the use of external high field NMR systems for polarizer calibrations or quality assurance of hyperpolarization compared to early polarizer designs [25; 26]. The estimated limit of detection of ^{13}C hyperpolarization for this RF probe is 1 micromole with 1% polarization in the 340 mL solenoid coil yielding a SNR > 8. Improving B_0 homogeneity and improving the RF circuit efficiency, which was outside the scope of this work, could further decrease this detection limit by as much as an order of magnitude.

^{13}C spectroscopy with the sodium 1-^{13}C-acetate phantom at 0.0475 T also enabled measurements of ^{13}C T_1 of the 1-^{13}C site in sodium acetate in low magnetic fields. It was found that T_1 =18.5 ± 0.8 s at ~50 μT (Earth field) and T_1 = 50.0 ± 2.6 s at 0.0475 T. Both values are significantly lower than the high field value for this phantom, ^{13}C T_1 = 70 s at 4.7 T (data not shown). This is in contrast with hyperpolarized HEP in H_2O, which has a significantly greater 1-^{13}C T_1 of 101 s at 0.0475 T [4] compared to 50 s at 4.7 T [26]. The magnetic field dependence of 1-^{13}C T_1 for acetate is different from the one for HEP. Hyperpolarized 1-^{13}C-pyruvate is a more advanced hyperpolarized contrast agent. It is also a carboxylic acid and therefore could exhibit a similar 1-^{13}C T_1 field trend. Therefore, the studies involving hyperpolarized material of carboxylic acids should avoid exposure to low fields in order to extend polarization lifetimes and preserve *in vitro* hyperpolarization as long as possible.

Achieving efficient hyperpolarization at sub-Watt RF power is very promising. The nominal cost is 10% reduction from the maximum observed polarization level at 10.5 W. The polarization losses at lower RF power are likely to be attributed to poorer excitation across the entire sample as B_1 becomes comparable to frequency distribution across the sample due to B_0 inhomogeneity or $B_1 \sim \Delta\omega_0$. The observed loss of polarization transfer efficiency is dominated more by losses associated with proton channel power level than with the ^{13}C channel losses. This is not surprising as $\Delta\omega_0(^1H) \sim 4\times\Delta\omega_0(^{13}C)$. This problem in the low power regime can be mitigated through additional improvement of RF coil B_1 efficiency and/or through the use of more homogeneous magnets. Nevertheless, using < 0.5 W power for ~10% hyperpolarization loss is a trade-off demonstrating the extent of possible device simplification due to reduced power requirements. Sub-watt RF amplifier used for PASADENA can be small and inexpensive, while increasing overall polarizer portability. Additionally, the entire polarizer setup can potentially be battery powered with use of a permanent B_0 magnet.

A relatively high sensitivity of low field detection of ^{13}C hyperpolarization is promising similarly to that of hyperpolarized noble gas for *in vivo* applications [17; 27]. While the low field SNR (Fig. 7B) is ~ 4 times lower than the 4.7 T signal (Fig. 7A), the effective line width due to worse B_0 homogeneity is also ~ 4 times greater and therefore the two spectra have similar integrated intensities. Solenoids are inherently more sensitive than the Litz design (Doty Scientific, SC), but our goal was to compare ultimate sensitivity of this low field device with a typical commercially available high field system. The renaissance of hyperpolarized MR makes this question worthy of reconsideration as low field MR may have favorable *in vivo* sensitivity. Although the induced *Emf* using field independent hyperpolarized magnetization is directly proportional to the resonant frequency ω_0, which is ~ 100 fold greater at 4.7 T compared to 0.0475 T, the low field ^{13}C coil has ~ 100 times greater turn density, largely compensating for the term $N{\cdot}\omega_0$ according to Faraday's law of induction (see Introduction). Thus, the similar 13C intensity detected from a simulated hyperpolarized state indicates that low field detection of hyperpolarized contrast agents can be of comparable sensitivity to that of high field. It should also be pointed out that low field MR sensitivity can be significantly improved by better magnet shimming and optimization/ improving of RF coil sensitivity (work in progress in our laboratory), which is outside the scope of this work, but would be critical for *in vivo* applications. Additional sensitivity could also be gained from indirect proton detection of hyperpolarized contrast agents [28; 29; 30] for spectroscopic and imaging applications [31].

The solenoid coil is a preliminary proof-of-principle design for primary use as a large volume RF coil for PHIP. Aiming for preclinical *in vivo* work with tumor bearing mice, the potential significant RF sensitivity improvements include: (i) decreasing RF coil volume by up to a factor of four leading to ~2 fold SNR gain, (ii) optimization of RF coil quality factor Q by increasing the turn density, wire thickness, and coil balancing with SNR expected gain ~2-5 fold, and (iii) cryogenic cooling (77 K) of the RF coil and preamplifier (SNR gain expected ~2-4 fold) [16]. The latter is technologically challenging for small animal imaging preclinical work, but perhaps would be more suitable for human imaging where additional SNR gain may be desired.

One of the main challenges for low field metabolic imaging of hyperpolarized contrast agents is diminishing chemical shift dispersion. This is especially challenging in relatively inhomogeneous B_0 field as the one used here. As a result, chemical shift phenomenon would be very difficult to exploit as a source of contrast in Chemical Shift Imaging (CSI) between parent and daughter molecules such as injected hyperpolarized 1-^{13}C-pyruvate and produced *in vivo* 1-^{13}C-lactate [32]. However, other mechanisms such as J-couplings can be potentially used to resolve multiple metabolites.

5. Conclusions

The presented 0.0475 T H-X probe for production of hyperpolarized contrast agents by PHIP has high MR sensitivity similar to that of conventional high field detection. It would potentially enable several low field NMR capabilities including sub-second imaging of ^{13}C and ^{15}N hyperpolarized contrast agents *in vivo* (work in progress in our laboratory). Direct *in situ* detection of low gamma nuclei permits precise, entirely self-contained pulse calibration of polarizing equipment producing ^{13}C and ^{15}N hyperpolarized contrast agents. The ability to quantify an external calibration standard with known concentration, MR signal, and polarization leads to better quality assurance of PHIP polarized contrast agents. Increased PHIP probe sensitivity and efficiency also enable PASADENA with sub-Watt RF power with ~10% loss of maximum producible hyperpolarization. Further optimization of RF coils should enable the use of low cost, small size and ultra-portable RF amplifiers for PHIP using low field magnets. However, we note that improvement of B_0 field homogeneity of low field magnets is at least as important as improving the RF coil performance [5].

The performance of the 0.0475 T H-X probe demonstrates sensitivity comparable to that of a 38 mm Doty volume coil of a 4.7 T small animal MRI scanner with respect to hyperpolarized contrast agents. Therefore, low field RF coils can have detection sensitivity similar to that of high field ones for hyperpolarized MR applications. Using multi-turn detection low field MR coils compensates signal losses arising from proportionality to detection frequency. These low field RF coils have vanishing restriction on the susceptibility concerns, specific absorption rate, and other limitations imposed by conventional high field MRI. However, the low limit of magnetic field and resonant detection frequency remains to be tested in the context of clinically sized RF coils.

Supplementary Material

Refer to Web version on PubMed Central for supplementary material.

Acknowledgments

We thank our funding sources: NIH R25 CA136440, NIH 5R00 CA134749-03, NIH 3R00CA134749-02S1, ICMIC 5P50CA128323-03.

References

[1]. Bowers CR, Weitekamp DP. Transformation of Symmetrization Order to Nuclear-Spin Magnetization by Chemical-Reaction and Nuclear-Magnetic-Resonance. Physical Review Letters. 1986; 57:2645–2648. [PubMed: 10033824]

[2]. Bowers CR, Weitekamp DP. Para-Hydrogen and Synthesis Allow Dramatically Enhanced Nuclear Alignment. Journal of the American Chemical Society. 1987; 109:5541–5542.

[3]. Shchepin RV, Coffey AM, Waddell KW, Chekmenev EY. PASADENA Hyperpolarized 13C Phospholactate. Journal of the American Chemical Society. 2012; 134:3957–3960. [PubMed: 22352377]

[4]. Waddell KW, Coffey AM, Chekmenev EY. In situ Detection of PHIP at 48 mT: Demonstration using a Centrally Controlled Polarizer. Journal of the American Chemical Society. 2011; 133:97–101. [PubMed: 21141960]

[5]. McDowell AF, Adolphi NL. Operating nanoliter scale NMR microcoils in a 1 tesla field. Journal of Magnetic Resonance. 2007; 188:74–82. [PubMed: 17627856]

[6]. Hoult DI, Richards RE. SIGNAL-TO-NOISE RATIO OF NUCLEAR MAGNETIC-RESONANCE EXPERIMENT. Journal of Magnetic Resonance. 1976; 24:71–85.

[7]. Hoult DI, Bhakar B. NMR signal reception: Virtual photons and coherent spontaneous emission. Concepts in Magnetic Resonance. 1997; 9:277–297.

[8]. Gor'kov PL, Chekmenev EY, Li CG, Cotten M, Buffy JJ, Traaseth NJ, Veglia G, Brey WW. Using low-E resonators to reduce RF heating in biological samples for static solid-state NMR up to 900 MHz. Journal of Magnetic Resonance. 2007; 185:77–93. [PubMed: 17174130]

[9]. Gor'kov PL, Witter R, Chekmenev EY, Nozirov F, Fu R, Brey WW. Low-E probe for F-19-H-1 NMR of dilute biological solids. Journal of Magnetic Resonance. 2007; 189:182–189. [PubMed: 17920316]

[10]. Michal CA. A low-cost spectrometer for NMR measurements in the Earth's magnetic field. Measurement Science & Technology. 2010; 21

[11]. Appelt S, Kuhn H, Hasing FW, Blumich B. Chemical analysis by ultrahigh-resolution nuclear magnetic resonance in the Earths magnetic field. Nature Physics. 2006; 2:105–109.

[12]. Bluemich B, Casanova F, Appelt S. NMR at low magnetic fields. Chemical Physics Letters. 2009; 477:231–240.

[13]. Halse ME, Coy A, Dykstra R, Eccles C, Hunter M, Ward R, Callaghan PT. A practical and flexible implementation of 3D MRI in the Earth's magnetic field. Journal of Magnetic Resonance. 2006; 182:75–83. [PubMed: 16828566]

[14]. Ledbetter MP, Theis T, Blanchard JW, Ring H, Ganssle P, Appelt S, Bluemich B, Pines A, Budker D. Near-Zero-Field Nuclear Magnetic Resonance. Physical Review Letters. 2011; 107

[15]. Meriles CA, Sakellariou D, Trabesinger AH, Demas V, Pines A. Zero- to low-field MRI with averaging of concomitant gradient fields. Proceedings of the National Academy of Sciences of the United States of America. 2005; 102:1840–1842. [PubMed: 15671161]

[16]. Darrasse L, Ginefri JC. Perspectives with cryogenic RF probes in biomedical MRI. Biochimie. 2003; 85:915–937. [PubMed: 14652180]

[17]. Parra-Robles J, Cross AR, Santyr GE. Theoretical signal-to-noise ratio and spatial resolution dependence on the magnetic field strength for hyperpolarized noble gas magnetic resonance imaging of human lungs. Medical Physics. 2005; 32:221–229. [PubMed: 15719973]

[18]. Abragam A, Goldman M. Principles of Dynamic Nuclear-Polarization. Reports on Progress in Physics. 1978; 41:395–467.

[19]. Perman WH, Bhattacharya P, Leupold J, Lin AP, Harris KC, Norton VA, Hoevener J-B, Ross BD. Fast volumetric spatial-spectral MR imaging of hyperpolarized (13)C-labeled compounds using multiple echo 3D bSSFP. Magnetic Resonance Imaging. 2011; 28:459–465. [PubMed: 20171034]

[20]. Park I, Bok R, Ozawa T, Phillips JJ, James CD, Vigneron DB, Ronen SM, Nelson SJ. Detection of Early Response to Temozolomide Treatment in Brain Tumors Using Hyperpolarized (13)C MR Metabolic Imaging. Journal of Magnetic Resonance Imaging. 2011; 33:1284–1290. [PubMed: 21590996]

[21]. Kurhanewicz J, Vigneron DB, Brindle K, Chekmenev EY, Comment A, Cunningham CH, DeBerardinis RJ, Green GG, Leach MO, Rajan SS, Rizi RR, Ross BD, Warren WS, Malloy CR. Analysis of Cancer Metabolism by Imaging Hyperpolarized Nuclei: Prospects for Translation to Clinical Research. Neoplasia. 2011; 13:81–97. [PubMed: 21403835]

[22]. Morris GA, Freeman R. Enhancement of Nuclear Magnetic-Resonance Signals by Polarization Transfer. Journal of the American Chemical Society. 1979; 101:760–762.

[23]. Feng B, Coffey AM, Colon RD, Chekmenev EY, Waddell KW. A pulsed injection parahydrogen generator and techniques for quantifying enrichment. Journal of Magnetic Resonance. 2012; 214:258–262. [PubMed: 22188975]

[24]. Goldman M, Johannesson H. Conversion of a proton pair para order into C-13 polarization by rf irradiation, for use in MRI. Comptes Rendus Physique. 2005; 6:575–581.

[25]. Hövener J-B, Chekmenev E, Harris K, Perman W, Robertson L, Ross B, Bhattacharya P. PASADENA hyperpolarization of 13C biomolecules: equipment design and installation. Magnetic Resonance Materials in Physics, Biology and Medicine. 2009; 22:111–121.

[26]. Hövener J-B, Chekmenev E, Harris K, Perman W, Tran T, Ross B, Bhattacharya P. Quality assurance of PASADENA hyperpolarization for 13C biomolecules. Magnetic Resonance Materials in Physics, Biology and Medicine. 2009; 22:123–134.

[27]. Patz S, Muradian I, Hrovat MI, Ruset IC, Topulos G, Covrig SD, Frederick E, Hatabu H, Hersman FW, Butler JP. Human pulmonary imaging and spectroscopy with hyperpolarized Xe-129 at 0.2T. Academic Radiology. 2008; 15:713–727. [PubMed: 18486008]

[28]. Chekmenev EY, Norton VA, Weitekamp DP, Bhattacharya P. Hyperpolarized (1)H NMR Employing Low gamma Nucleus for Spin Polarization Storage. Journal of the American Chemical Society. 2009; 131:3164–3165. [PubMed: 19256566]

[29]. Sarkar R, Comment A, Vasos PR, Jannin S, Gruetter R, Bodenhausen G, Hall H, Kirik D, Denisov VP. Proton NMR of N-15-Choline Metabolites Enhanced by Dynamic Nuclear Polarization. Journal of the American Chemical Society. 2009; 131:16014. + [PubMed: 19848401]

[30]. Pfeilsticker JA, Ollerenshaw JE, Norton VA, Weitekamp DP. A selective N-15-to-H-1 polarization transfer sequence for more sensitive detection of N-15-choline. Journal of Magnetic Resonance. 2010; 205:125–129. [PubMed: 20472478]

[31]. Harris T, Giraudeau P, Frydman L. Kinetics from Indirectly Detected Hyperpolarized NMR Spectroscopy by Using Spatially Selective Coherence Transfers. Chemistry-a European Journal. 2011; 17:697–703.

[32]. Yen YF, Kohler SJ, Chen AP, Tropp J, Bok R, Wolber J, Albers MJ, Gram KA, Zierhut ML, Park I, Zhang V, Hu S, Nelson SJ, Vigneron DB, Kurhanewicz J, Dirven H, Hurd RE. Imaging Considerations for In Vivo C-13 Metabolic Mapping Using Hyperpolarized C-13-Pyruvate. Magnetic Resonance in Medicine. 2009; 62:1–10. [PubMed: 19319902]

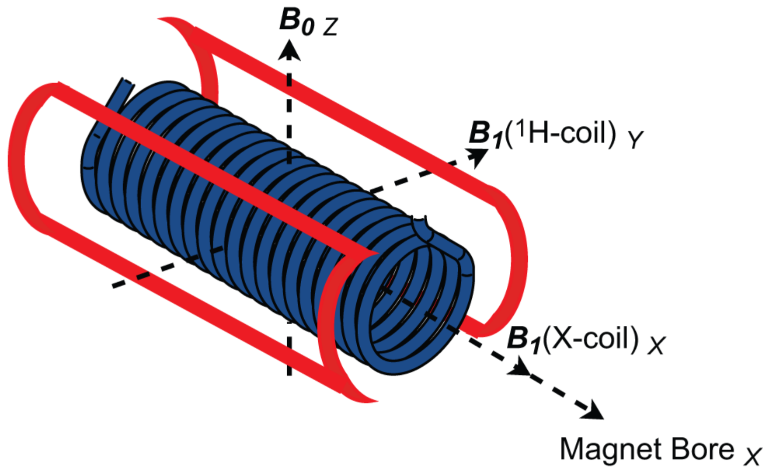

Fig. 1.
Alignment of RF coils, magnetic field and magnet bore.

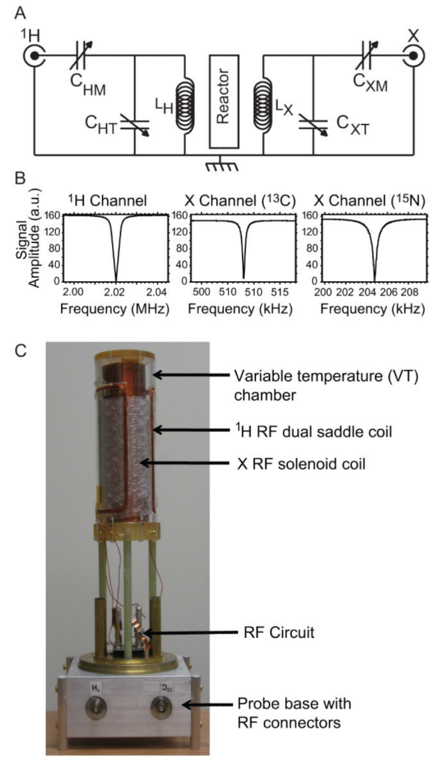

Fig. 2.

NMR Probe RF Circuit. (A) The RF design consists of two single channel circuits with common ground tuned for ^{1}H at the high frequency and $^{13}C/^{15}N$ at the low frequency. (B) Frequency sweep response showing ^{1}H circuit resonating at 2.02 MHz, ^{13}C at 0.508 MHz, and ^{15}N at 0.205 MHz. (C) The NMR probe design.

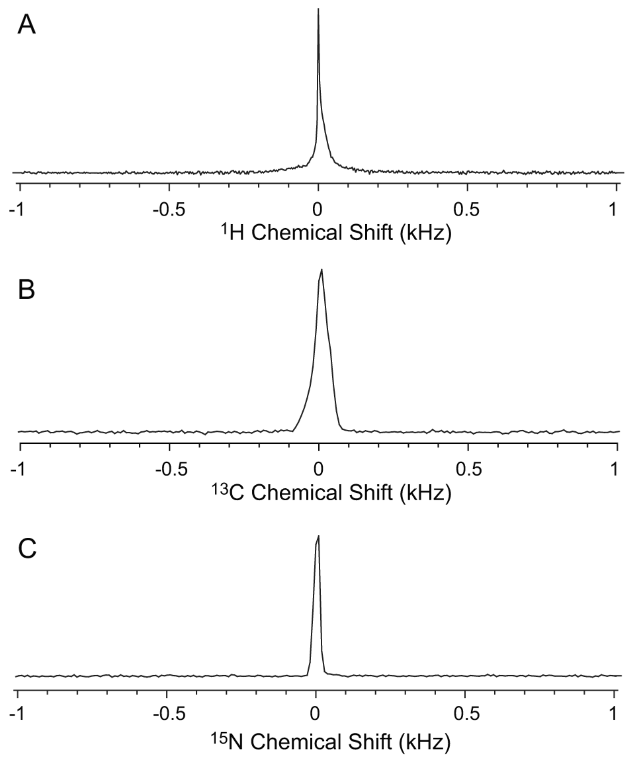

Fig. 3.

NMR spectroscopy at 0.0475 T. (A) Single scan ^{1}H spectrum of aqueous 5 mM $CuSO_4$ 24 mL. (B) Single scan ^{13}C NMR spectrum of 42 mL of 3M solution (0.13 moles or 11 g) sodium 1-^{13}C-acetate solution in 99.8% D_2O acquired after sample pre-polarization at 4.7 T and ~ 7 s long transfer at Earth field. (C) Single scan ^{15}N NMR spectrum of 48 mL of 4.6 M (0.22 moles or 12 g) of $^{15}NH_4Cl$ in 99.8% D_2O after sample pre-polarization at 7 T and ~ 7 s long transfer at Earth field. All spectra are acquired with 90° excitation RF pulse.

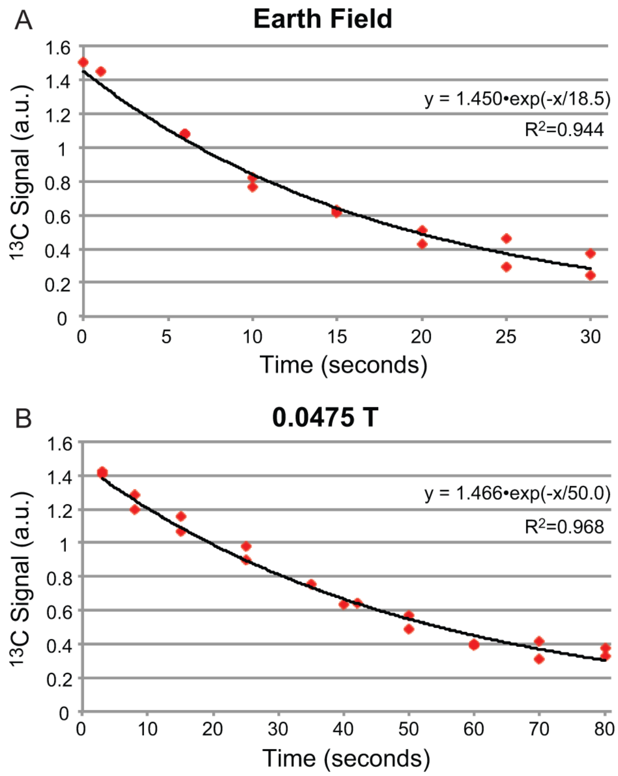

Fig. 4.
^{13}C T_1 measurements for sodium 1-^{13}C-acetate in 99.8% D_2O (A) at Earth field of ~50 μT yielding ^{13}C $T_1 = 18.5 \pm 0.8$ s, and (B) at $B_0 = 0.0475$ T yielding ^{13}C $T_1 = 50.0 \pm 2.6$ s.

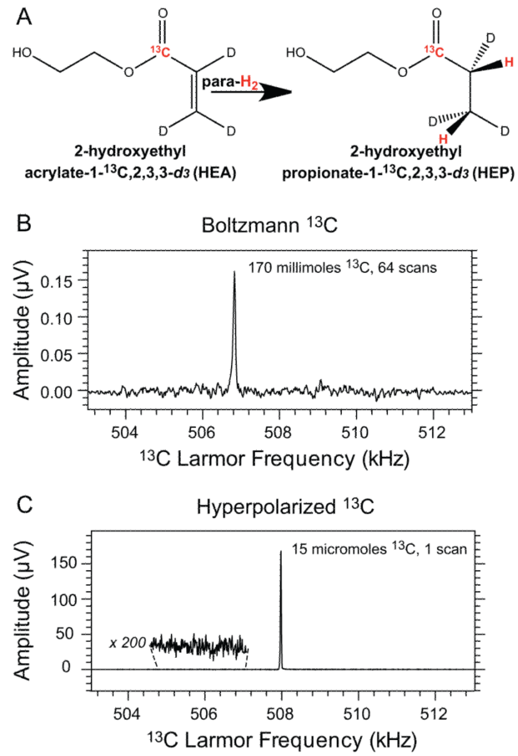

Fig. 5.

PHIP hyperpolarization of HEP. **(**A) Conversion of HEA to HEP via molecular addition of parahydrogen in the PHIP process leading to hyperpolarization of the 1-^{13}C carbon (red). (B) ^{13}C spectroscopy of a 60 mL of 2.8 M ^{13}C reference sample containing 0.17 moles or 14 g of sodium 1-^{13}C-acetate using Boltzmann polarization and 64 averages. (C) Single acquisition spectrum of 15 micromoles (< 2 mg) of hyperpolarized HEP contrast agent with 20% polarization or enhancement **ε** ~ 5,000,000 at 0.0475 T.

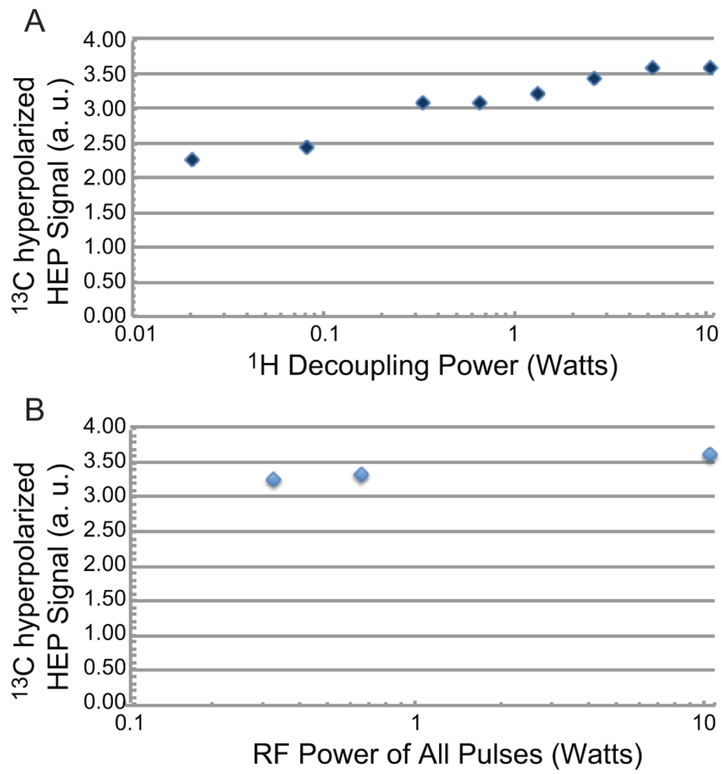

Fig. 6.
Dependence of ^{13}C hyperpolarized signal on RF excitation pulse power. (A) Effect of ^{1}H decoupling power on ^{13}C hyperpolarized signal (arbitrary units) of HEP using 10.5 W power for RF transfer pulses. (B) ^{13}C hyperpolarized signal (arbitrary units) of HEP dependence on power level of PHIP RF pulses where power of all RF pulses is incremented.

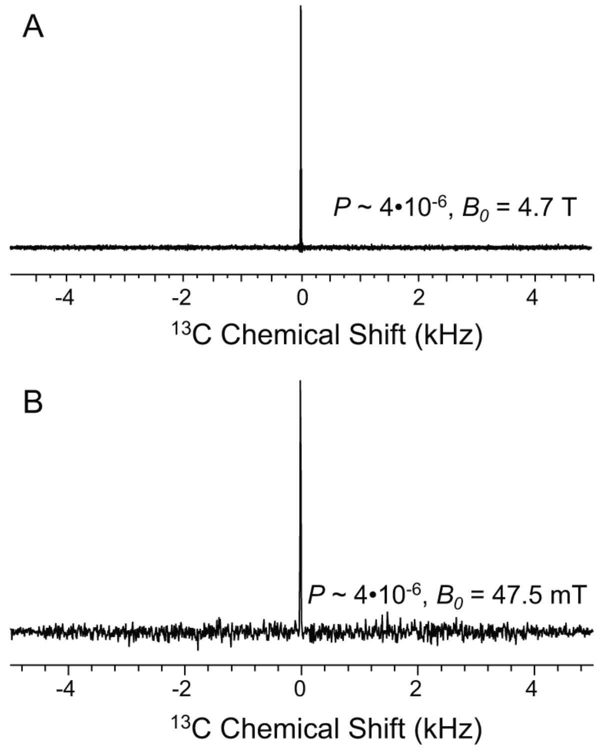

Fig. 7.

B>. Sensitivity comparison at high and low field. ^{13}C spectroscopy of 2.8 mL of 4.3 M (0.012 moles or 1.0 g) of sodium 1-^{13}C-acetate solution in 99.8% D_2O at (A) 4.7 T with SNR = 120 using multinuclear RF coil (Doty Scientific, SC) and at (B) 0.0475 T with SNR = 30 using the H-X RF coil for acquisition ~7 s after pre-polarization at 7 T to render ^{13}C polarization equivalent to Boltzmann polarization at 4.7 T. Both spectra used spectral width = 10 kHz, no line broadening and other similar acquisition parameters.

Table 1

RF circuit component values and performance parameters.

Channel	Capacitor	Values (pF)	Inductor	Value (μH)	τ_{90}° / Power	B_1 (kHz) / Power
^{1}H	C_{TH}	0-120 variable	L_H	40	86 μs / 5.3 W	2.9 kHz / 5.3 W
	C_{MH}	0-20 variable + 68 fixed				
^{13}C	C_{XT}	0-120 variable	L_X	550	62 μs / 5.3 W	4.0 kHz / 5.3 W
	C_{XM}	0-120 variable + 56 fixed				
^{15}N	C_{XT}	0-120 variable + 940 fixed			73 μs / 10.5 W	3.4 kHz / 10.5 W
	C_{XM}	0-120 variable + 384 fixed				